High-energy neutrino fluxes and flavor ratio in the Earth's atmosphere

T. S. Sinegovskaya,[1] A. D. Morozova,[2] and S. I. Sinegovsky[3,*]

[1]*Irkutsk State Railway University, 664074 Irkutsk, Russia*
[2]*Physics Faculty, Irkutsk State University, 664003 Irkutsk, Russia*
[3]*Institute of Applied Physics, Irkutsk State University, 664003 Irkutsk, Russia*

We calculate the atmospheric neutrino fluxes in the energy range 100 GeV–10 PeV with the use of several known hadronic models and a few parametrizations of the cosmic-ray spectra which take into account the knee. The calculations are compared with the atmospheric neutrino measurements by Frejus, AMANDA, IceCube, and ANTARES. An analytic description is presented for the conventional $(\nu_\mu + \bar{\nu}_\mu)$ and $(\nu_e + \bar{\nu}_e)$ energy spectra, averaged over zenith angles, which can be used to obtain test data of the neutrino event reconstruction in neutrino telescopes. The sum of the calculated atmospheric ν_μ flux and the IceCube best-fit astrophysical flux gives the evidently higher flux as compared to the IceCube59 data, giving rise the question concerning the hypothesis of the equal flavor composition of the high-energy astrophysical neutrino flux. Calculations show that the transition from the atmospheric electron neutrino flux to the predominance of the astrophysical neutrinos occurs at 30–100 TeV if the prompt neutrino component is taken into consideration. The neutrino flavor ratio, extracted from the IceCube data, does not tend to increase with the energy as is expected for the conventional neutrino flux in the energy range 100 GeV–30 TeV. A depression of the ratio R_{ν_μ/ν_e} possibly indicates that the atmospheric electron neutrino flux obtained in the IceCube experiment contains an admixture of the astrophysical neutrinos in the range 10–50 TeV.

I. INTRODUCTION

High-energy neutrinos produced in decays of pions, kaons, and charmed particles of the extensive air shower, induced by cosmic rays passing through the Earth's atmosphere, form an unavoidable background for the detection of astrophysical neutrinos. Sources of extra-terrestrial high-energy neutrinos is the challenge to solve which the large-scale neutrino telescopes, NT200+ [1], IceCube [2–4], ANTARES [5,6] are designed. The high-energy atmospheric neutrinos became accessible for exper-imental studies only in recent years. The energy spectrum of high-energy atmospheric muon neutrinos has been measured in the following four experiments: Frejus [7] at energies up to 1 TeV, AMANDA-II [8] in the energy range 1–100 TeV, IceCube [2,9] at 100 GeV–575 TeV, and ANTARES at energies 100 GeV–200 TeV [5]. Not long ago, IceCube also presented results for the electron neutrino spectrum measured in the energy range ∼80 GeV–6 TeV [10]. Thus, a possibility appeared for evaluating the neutrino flavor ratio using the IceCube measurements and comparing this one with predictions.

Lately IceCube found the 37 high-energy neutrino events [11–13] in the energy range 30 TeV–2 PeV, most of which are hardly consistent with events expected from the atmospheric muons and neutrinos, 8.4 ± 4.2 and $6.6^{+5.9}_{-1.6}$, respectively. The neutrino events, three of which have

energies above 1 PeV, were detected over the three years 2010–2013 (988 days), give the statistical significance of their astrophysical origin at the level of 5.7σ.

After the IceCube reported [11] on the detection of the first two neutrino-induced events with deposited energy 1.04 and 1.14 PeV, the prompt analysis of the origin of the highest energy neutrinos ever detected was performed [14–21].

Increasing with energy contribution of charmed particles to the atmospheric neutrino flux becomes the source of the large uncertainty at energies above ∼200 TeV for muon neutrinos and above ∼20 TeV for electron neutrinos. A more complicated picture is likely if the astrophysical neutrinos and the atmospheric conventional or prompt ones are entangled. It is quite possible that astrophysical neutrino flux becomes dominant over the atmospheric electron neutrino flux at energies 20–50 TeV. Thus, a comparison of atmospheric neutrino spectra calculated for various hadron-interaction models with high-energy neutrino spec-tra measurements can shed light on the most uncertain constituent of the atmospheric neutrino background, in spite of large statistical and systematic uncertainties.

Here we calculate atmospheric neutrino fluxes at ener-gies $10^2 - 10^7$ GeV for zenith angles from 0° to 90° as well as the angle-averaged spectrum with the use of high-energy hadronic interaction models QGSJET II-03 [22] and SIBYLL 2.1 [23]. These models are widely employed to simulate extensive air showers (EAS) with the Monte Carlo method and were also applied to compute the cosmic-ray

*sinegovsky@api.isu.ru

hadron and muon fluxes [24,25]. Besides, in this work computation we employ also the old known hadronic model by Kimel and Mokhov (KM) [26] which was checked by comparison of the calculated atmospheric hadron and muon spectra with the experiment [24].

The calculation has been performed for three parametrizations of the measured spectra and composition of primary cosmic rays in the energy range comprising the knee: (i) the model by Zatsepin and Sokolskaya (ZS) [27], (ii) the model by Hillas [28] and Gaisser (HGm) [29], and (iii) the modified multiknee (polygonato) model (BK) [30,31]. Below we denote, for short, different versions of the calculations according to the pattern "a primary cosmic-ray spectrum + an hadronic interaction model" or, vice versa, "an hadronic interaction model + a primary cosmic-ray spectrum," for example, HGm + QGSJET (or HGm + QGS2), ZS + QGS2, HGm + KM, SIBYLL + BK, and so on.

The paper is organized as follows. In Sec. II we give a sketch of the computation scheme: a short review of the calculation method and the data input, primary cosmic-ray spectra, and hadronic interaction models used in the computation. In Sec. III we present the results of the calculation of the atmospheric muon neutrino energy spectrum and a comparison with experiments. In Sec. IV we compare calculations of the electron neutrino spectrum and the neutrino flavor ratio R_{ν_μ/ν_e} with the IceCube measurements. The main results of the paper are discussed in Sec. V.

II. SCHEME OF THE COMPUTATION

A. Outline of the calculation method

To compute the atmospheric muon and electron neutrino spectra, we employ the method to solve the hadronic cascade equations [24,32], which makes it possible to consider the nonpower behavior of the cosmic-ray spectrum, energy-dependent total inelastic cross sections $\sigma_{hA}^{in}(E)$ of hadron-nucleus interactions, and a violation of the Feynman scaling law for the inclusive cross sections. The calculation procedure was validated through the careful comparison with experiments of the calculated atmospheric hadron fluxes and the sea-level muon spectrum which covers the wide range of energies for different zenith angles [24,25]. Omitting details, we give here a brief review of the calculation scheme aimed to introduce generalized Z factors.

The differential energy spectra of the secondary protons $p(E,h)$ and neutrons $n(E,h)$ at atmospheric depth h obey the equations

$$\frac{\partial N^\pm(E,h)}{\partial h} = -\frac{N^\pm(E,h)}{\lambda_N(E)} + \frac{1}{\lambda_N(E)}$$
$$\times \int_0^1 \Phi_{NN}^\pm(E,x) N^\pm(E/x,h)\frac{dx}{x^2}, \quad (1)$$

where $N^\pm(E,h) = p(E,h) \pm n(E,h)$,

$$\Phi_{NN}^\pm(E,x) = \frac{E}{\sigma_{pA}^{in}(E)}\left[\frac{d\sigma_{pp}(E_0,E)}{dE} \pm \frac{d\sigma_{pn}(E_0,E)}{dE}\right],$$

$\lambda_N(E) = [N_0\sigma_{pA}^{in}(E)]^{-1}$ is the nucleon interaction length, $N_0 = N_A/A$ is the number of nuclei per gram of air, $x = E/E_0$ is the fraction of the primary nucleon energy E_0 carried away by the secondary nucleon, $d\sigma_{ab}/dE$ is a cross section for the inclusive reaction $a + A \rightarrow b + X$, integrated over the transverse momentum. The boundary conditions for Eq. (1) are $N^\pm(E,0) = p_0(E) \pm n_0(E)$.

Let us seek a solution of system (1) in the form

$$N^\pm(E,h) = N^\pm(E,0)\exp\left[-\frac{h(1 - \mathcal{Z}_{NN}^\pm(E,h))}{\lambda_N(E)}\right], \quad (2)$$

where $\mathcal{Z}_{NN}^\pm(E,h)$ are unknown functions. Substitution of Eq. (2) into (1) yields equations for the functions $\mathcal{Z}_{NN}^\pm$ ($\mathcal{Z}$ factors),

$$\frac{\partial(h\mathcal{Z}_{NN}^\pm)}{\partial h} = \int_0^1 dx\Phi_{NN}^\pm(E,x)\eta_{NN}^\pm(E,x)$$
$$\times \exp\left[-h\mathcal{D}_{NN}^\pm(E,x,h)\right], \quad (3)$$

where $\eta_{NN}^\pm(E,x) = x^{-2}N^\pm(E/x,0)/N^\pm(E,0)$,

$$\mathcal{D}_{NN}^\pm(E,x,h) = \frac{1 - \mathcal{Z}_{NN}^\pm(E/x,h)}{\lambda_N(E/x)} - \frac{1 - \mathcal{Z}_{NN}^\pm(E,h)}{\lambda_N(E)}. \quad (4)$$

Integrating Eq. (3), one obtains a nonlinear integral equation,

$$\mathcal{Z}_{NN}^\pm(E,h) = \frac{1}{h}\int_0^h dt \int_0^1 dx\Phi_{NN}^\pm(E,x)\eta_{NN}^\pm(E,x)$$
$$\times \exp\left[-t\mathcal{D}_{NN}^\pm(E,x,t)\right], \quad (5)$$

which we solve using the iterative approach. Choosing as the starting point $\mathcal{Z}_{NN}^{\pm(0)}(E,h) = 0$, i.e., $\mathcal{D}_{NN}^{\pm(0)}(E,x,h) = 1/\lambda_N(E/x) - 1/\lambda_N(E)$, we find for the nth step

$$\mathcal{Z}_{NN}^{\pm(n)}(E,h) = \frac{1}{h}\int_0^h dt \int_0^1 dx\Phi_{NN}^\pm(E,x)\eta_{NN}^\pm(E,x)$$
$$\times \exp\left[-t\mathcal{D}_{NN}^{\pm(n-1)}(E,x,t)\right], \quad (6)$$

$$\mathcal{Z}_{NN}^{\pm(n)}(E,h) = \frac{1}{h}\int_0^h dt \int_0^1 dx\Phi_{NN}^\pm(E,x)\eta_{NN}^\pm(E,x)$$
$$\times \exp\left[-t\mathcal{D}_{NN}^{\pm(n-1)}(E,x,t)\right], \quad (7)$$

where

$$\mathcal{D}_{NN}^{\pm(n-1)}(E,x,h) = \frac{1 - \mathcal{Z}_{NN}^{\pm(n-1)}(E/x,h)}{\lambda_N(E/x)}$$
$$- \frac{1 - \mathcal{Z}_{NN}^{\pm(n-1)}(E,h)}{\lambda_N(E)}. \qquad (8)$$

The functions $\mathcal{Z}(E,h)$ depend on two variables unlike the commonly known z factor and carry imprints of cosmic-ray spectra, hadron-nuclei interactions, and the hadronic cascade evolution in the atmosphere. In the case of the power-law, cosmic-ray spectrum, the Feynman scaling for the hadron production cross sections and $\sigma_{hA}^{in} = $ const, the function $\mathcal{Z}_{ab}(E,h)$ is reduced to a constant or $z_{ab}(E)$ (see details in Refs. [25,33]).

In a similar fashion, meson cascade equations can be solved using the nucleon and meson sources [24]. The main pion sources in the atmospheric shower are the interactions of nucleons and pions with air nuclei and kaon decays. As a first step, the meson component can be detached from the nucleon one by neglecting the small contribution from the $N\bar{N}$ pair production in meson-nucleus collisions. At this step, the pion equations are detached from the kaon ones with neglect of kaon decays to pions as well as of the pion production by kaons. In turn, the kaon part of the cascade contains the nucleon source as the main one and pion sources as additional sources in as much as the reaction $\pi + A \to K + X$ is taken into account.

At the second step, one can calculate small corrections to the nucleon, pion, and kaon fluxes, allowing for (i) additional pion sources from decays of kons to pions, (ii) pion production in kaon-nuclei collisions, $K + A \to \pi + X$, and (iii) $N\bar{N}$ pair production.

The Genz-Malik adaptive cubature algorithm [34] turned out to be very useful in a numerical realization of the method for multidimensional integration; a fast algorithm based on quadratic B-splines was used to interpolate and approximate the calculated functions. Note the high convergence of the method: in the nucleon component calculations, five iterations are required to achieve an accuracy close to 1%, while two iterations are enough to achieve the same accuracy in the meson flux computations.

B. Primary cosmic-ray spectra

As the primary cosmic-ray spectra and composition in the wide-energy range, we use in our calculations the following models: (1) the model by Zatsepin and Sokolskaya (ZS), (2) the novel cosmic-ray (CR) spectrum approximation (HGm) by Hillas [28] and Gaisser [29], and (3) the modified multiknee model by Bindig, Bleve, and Kampert (BK) [30] based on KASCADE data [35] and the polygonato model by Hörandel [31].

The Zatsepin and Sokolskaya model [27] comprises contributions to the cosmic-ray flux of three classes of Galaxy astrophysical sources: (I) isolated (nonassociated) supernovae (SNe) exploding into random interstellar

medium (ISM), the magnetic rigidity $R = E_{CR}/eZ < 50$ TV; (II) the most powerful sources of CR, which are high mass SNe exploding into ISM in OB associations that give rise to particles with energies up to $4Z$ PeV: CR particles are accelerated by shock waves passing through the stellar wind, i.e., OB star explodes into a dense ISM; (III) weak sources owing to explosions of novae, $R < 200$ GV.

All three classes of CR sources produce power-law energy spectra with different spectral indices, $\gamma = \alpha + 0.33$, where α is the index of source spectrum. In the region of effective acceleration, spectral indices are 2.63 (class I), 2.43 (II), and 2.90 (III). In the energy range $E = 100$ TeV $- 1$ PeV, fluxes of p and He rise ($\gamma_{p;He} < 2.75$), median nuclei (CNO) and heavy ones fall ($\gamma_{CNO} > 2.75$). At the energies above the CR "knee" ($E > 3$ PeV) p and He diminish, and heavy nuclei grow. Fe nuclei dominate at $E > 30$ PeV.

The model ZS describes well data of the ATIC2 direct measurements [36] in the range 10–10^5 GeV and gives a motivated extrapolation of these data up to 100 PeV—the energy region where the cosmic-ray spectra and elemental composition are derived from measured characteristics of EAS. The ZS proton and helium spectra at $E \gtrsim 10^6$ GeV are compatible with KASCADE spectra, reconstructed with the usage of hadronic models QGSJET01 and SIBYLL. ZS spectra well agree also with the Hillas-Gaisser model up to 1 PeV.

Since direct measurements of the cosmic-ray spectra and elemental composition are terminated close to 100 TeV, one needs to make the spectrum extrapolation to high energies, above the knee. The model by Hillas and Gaisser [28,29] includes three classes of sources: (i) supernova remnants in the Galaxy, (ii) Galaxy high-energy sources of still uncertain origin which contribute to the cosmic-ray flux between the "knee" (3 PeV) and the "ankle" (4 EeV), and (iii) extragalactic astrophysical objects (Active Galactic Nuclei, sources of the gamma-ray bursts, and others).

The composite spectrum is formed of five groups of nuclei (p, He, CNO, Mg-Si, and Mn-Fe). Each of the three populations accelerates five groups of nuclei, the spectrum of which cuts off at a characteristic rigidity. The parameters for the class (i) spectrum were taken from CREAM measurements [37] and extrapolated (to a rigidity of 4 PV) to take into account the knee. The extrapolation is consistent with measurements of the all-particle spectrum beyond the knee in the EAS experiments. The extragalactic component also takes into account the measurement data by HiRes, PAO, and Telescope Array. In our calculations, we use the version with mixed composition for extragalactic sources of cosmic rays, denoted here as HGm, which corresponds to the H3a of Ref. [38]. More details concerning this parametrization can be found in Ref. [39].

The polygonato model [31] comprising only galactic sources is the third known cosmic-ray model used in our calculations. The modified multiknee (polygonato) model

by Bindig, Bleve, and Kampert [30] was aimed to take into account the KASCADE data [35] concerning elemental composition of cosmic rays around the knee.

C. High-energy hadronic interaction models

Calculations of hadronic cascades induced by high-energy cosmic-ray particles and the atmospheric neutrino flux of the PeV scale require either an extrapolating cross section measured at lower energies or developing the models to give the reliable predictions at high and ultrahigh energies. Direct measurements of inclusive cross sections for the nucleon and meson production in hadron-nucleus collisions are still far from being complete because of the restricted kinematics region of the LHC cross section measurements.

In this work, we apply known hadronic interaction models QGSJET II-03 [22] and SIBYLL 2.1 [23], which currently undergo overall tests in two ways: (i) through simulations of EAS induced by high-energy cosmic-ray particles and (ii) through comparison of the model predictions with results of LHC experiments.

Besides, we also use the hadronic interaction model proposed by Kimel and Mokhov (KM) [26], for which we adopt updated parameters [32,40,41]. Based on accelerator data at energies up to 1.5 TeV, KM however obeys the Feynman scaling law and can be valid for higher energies, making predictions compatible with QGSJET and SIBYLL. The predictions of the KM model for pp and pA interactions are also close to the results obtained in the hadronic model DPMJET-III [42,43], based (like SIBYLL) on the dual parton model. The KM model was also applied in three-dimensional Monte Carlo calculations of the atmospheric neutrino fluxes [44].

The current models differ in accuracy of description of soft interactions and contribution of the diffraction dissociation, in ways to account for semihard interactions (minijets), in description of hadron-nucleus interactions (Glauber approach or Glauber-Gribov theory, the

superposition or semisuperposition picture), in the degree of the scaling violation at high energies.

To illustrate in part the difference of the hadronic models one can compute the cosmic-ray spectrum-weighted moments (z factors) for proton-air interactions $pA \to cX$ of the inclusive spectra $(x/\sigma_{pA}^{in})(d\sigma_{pc}/dx)$:

$$z_{pc}(E_0) = \int_0^1 \frac{x^\gamma}{\sigma_{pA}^{in}} \frac{d\sigma_{pc}}{dx} dx, \qquad (9)$$

where $x = E_c/E_0$, $\gamma = 1.7$, $c = \pi^\pm$, $K^\pm$; z factors for DPMJET-III are borrowed from Ref. [43]. As one can see from Table I, z factors obey the approximate scaling law in DPMJET-III, KM, and SIBYLL 2.1 (except the production of K mesons), while in the case of QGSJET-II, noticeable violation of the scaling is found just for pions.

III. FLUXES OF ATMOSPHERIC MUON NEUTRINOS

The calculation is performed on the basis of the method [24,32] of the solution of the hadronic cascade equations in the atmosphere, taking into account the nonpower energy spectrum of the cosmic rays, a violation of Feynman scaling, and a growth with the energy of the total inelastic cross sections of hadron-nucleus collisions.

Along with the major sources of the muon neutrinos, the $\pi_{\mu 2}$ and $K_{\mu 2}$ decays, we consider three-particle semileptonic decays of charged and neutral kaons, $K_{\mu 3}^\pm$ (the branching ratio 3.32%), $K_{\mu 3}^0$ (27%). Moreover we account for small contributions originating from decay chains $K \to \pi \to \nu_\mu$ ($K_S^0 \to \pi^+\pi^-$, $K^\pm \to \pi^\pm\pi^0$), and from the muon decays.

The comparison of the muon neutrino fluxes calculated with three recent primary spectrum models (Fig. 1) shows that they are rather close to each other up to 1 PeV. In Table II presented are neutrino flux ratios (averaged over zenith angles) calculated with usage of three hadronic models QGSJET-II, SIBYLL and KM: columns marked as 1,2,3 present comparative $(\nu_\mu + \bar\nu_\mu)$ fluxes, $\phi_{\nu_\mu}^{(\text{SIBYLL})}/\phi_{\nu_\mu}^{(\text{QGSJET II})}$, $\phi_{\nu_\mu}^{(\text{KM})}/\phi_{\nu_\mu}^{(\text{QGSJETII})}$, and $\phi_{\nu_\mu}^{(\text{SIBYLL})}/\phi_{\nu_\mu}^{(\text{KM})}$ respectively. Columns 4,5,6 give the same for the conventional $\nu_e + \bar\nu_e$ flux. All computations are performed for ZS and HGm cosmic-ray spectra. One can see that QGSJET-II and SIBYLL 2.1 lead to apparent difference in the muon neutrino flux, as well as in the case of SIBYLL as compared to KM. However with the energy rise the flux difference between SIBYLL and KM predictions diminishes, so that at energies above 100 TeV these fluxes are in close agreement. Quite contrary, the QGSJET-II and KM flux difference becomes notable just above 100 TeV.

In Figs. 2 and 3, the conventional $\nu_\mu + \bar\nu_\mu$ fluxes averaged over zenith angles in the range 96°–180° (the upward neutrinos, $\cos\theta \lesssim -0.1$), calculated with use of ZS and BK spectra, are compared with Frejus [7], AMANDA-II

TABLE I. z_{pc} factors for π and K mesons.

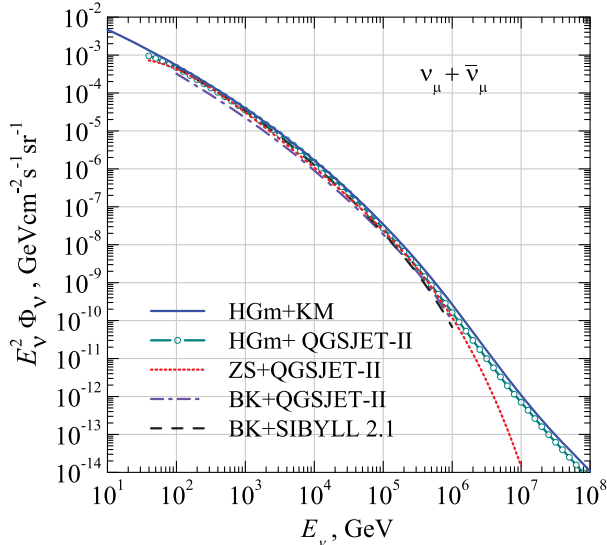| Model	E_0, GeV	$z_{p\pi^+}$	$z_{p\pi^-}$	z_{pK^+}	z_{pK^-}
	10^2	0.043	0.035	0.0036	0.0030
QGSJET	10^3	0.036	0.029	0.0036	0.0028
II-03	10^4	0.033	0.028	0.0034	0.0027
	10^2	0.036	0.026	0.0134	0.0014
SIBYLL	10^3	0.038	0.029	0.0120	0.0023
2.1	10^4	0.037	0.029	0.0097	0.0027
	10^2	0.044	0.027	0.0051	0.0015
KM	10^3	0.046	0.028	0.0052	0.0015
	10^4	0.046	0.029	0.0052	0.0015
DPMJET	10^3	0.04	0.035	0.0070	0.0035
III	10^4	0.04	0.035	0.0070	0.0031

FIG. 1 (color online). Comparison of atmospheric $\nu_\mu + \bar{\nu}_\mu$ fluxes calculated using three hadronic models, KM, QGSJET-II-03, SIBYLL 2.1, and three parametrizations of the cosmic-ray spectrum.

[8], and IceCube40 [2] measurement data obtained with the 40-string configuration of the IceCube detector.

To illustrate the influence of the "knee" in the cosmic-ray spectrum, in Fig. 2 we plot also the conventional ($\nu_\mu + \bar{\nu}_\mu$) spectrum computed with usage of the cosmic-ray parametrization by Gaisser, Honda, Lipari and Stanev (GH) [45]. The right panel of Fig. 2 shows an influence of the hadronic models, QGSJET vs SIBYLL (see also Table II). The difference in the neutrino flux predictions resulted from cosmic-ray spectra becomes apparent at high neutrino energies: the flux obtained for GH spectrum at 600 TeV is nearly twice as large as that for ZS spectrum for the same hadronic model. Close to 1 PeV, this discrepancy increases to factor of 5. More results concerning the muon neutrino

TABLE II. The neutrino flux ratio calculated with SIBYLL 2.1, QGSJET-II-03 and KM for cosmic-ray spectra ZS [27] and HGm [29]: sib/qgs2–column 1 (4); km/qgs2–2 (5); sib/km–3 (6).

E_ν, GeV	1	2	3	4	5	6
	ZS: ($\nu_\mu + \bar{\nu}_\mu$)			ZS: ($\nu_e + \bar{\nu}_e$)		
10^3	1.70	1.05	1.62	1.48	0.85	1.74
10^4	1.53	1.04	1.47	1.39	0.81	1.72
10^5	1.53	1.10	1.39	1.35	0.95	1.42
10^6	1.79	1.64	1.09	1.48	1.56	0.96
10^7	1.85	2.08	0.89	1.45	1.91	0.76
	HGm: ($\nu_\mu + \bar{\nu}_\mu$)			HGm: ($\nu_e + \bar{\nu}_e$)		
10^3	1.59	0.85	1.87	1.45	0.81	1.79
10^4	1.57	1.12	1.40	1.41	0.85	1.65
10^5	1.57	1.27	1.24	1.38	1.01	1.37
10^6	1.63	1.63	1.00	1.37	1.27	1.08
10^7	1.47	1.53	0.96	1.28	1.10	1.17

calculations compared to the AMANDA and IceCube40 measurements were presented in Refs. [46–48].

The prompt neutrino flux was calculated using the quark-gluon string model (QGSM) by Kaidalov & Piskunova [49,50] as well as the recombination quark-parton model (RQPM) [50]. In Fig. 3 the prompt neutrino calculations were performed with the parametrization of the cosmic-ray spectrum by Nikolsky, Stamenov and Ushev (NSU) [51], therefore they can serve here as upper limits for the prompt neutrino flux due to QGSM or RQPM.

Addition of the QGSM prompt contribution evidently improves the agreement of the calculation example ZS + QGSJET with the IceCube40 measurement data [2] above 100 TeV. The prompt neutrino flux due to QGSM and RQPM can be approximated at energies 5 TeV $\leq E \leq 5$ PeV by the expressions

$$\phi_\nu^{(\text{qgsm})}(E) = A(E/E_1)^{-3.01}[1 + (E/E_1)^{-2.01}]^{-0.165}, \quad (10)$$

$$\phi_\nu^{(\text{rqpm})}(E) = B(E/E_1)^{-2.96}[1 + (E/E_1)^{-1.96}]^{-0.157}, \quad (11)$$

where $A = 1.19 \times 10^{-18}$, $B = 4.65 \times 10^{-18}$ $(\text{GeV} \, \text{cm}^2 \, \text{s} \, \text{sr})^{-1}$, $E_1 = 100$ TeV.

Figure 4 shows calculations of the atmospheric muon neutrino spectrum in comparison with the measurement data obtained in recent experiments, IceCube40 [2], ANTARES [5] and IceCube59 [9]. In Ref. [9] results were presented of the novel reconstruction of the muon neutrino spectrum with use of the data obtained with the 59-string IceCube configuration. The calculations of the conventional flux were performed for a set of models: HGm + QGSJET-II (red solid line), HGm + SIBYLL (magenta), HGm + KM (blue bold dots), ZS + QGSJET-II (dashed line). The QGSM and RQPM prompt neutrino fluxes obtained [50] with NSU spectrum are shown separately (short dash and dash-dot lines, respectively). The total atmospheric ($\nu_\mu + \bar{\nu}_\mu$) spectrum was calculated with the model HGm + QGSJET + QGSM (blue solid line).

The conventional flux due to the HGm + QGSJET is similar to that of ZS + QGSJET up to 1 PeV. The difference of the neutrino flux predictions originated from the primary cosmic-ray spectra becomes apparent above 1 PeV: the flux obtained with QGSJET-II for ZS spectrum at 2 PeV is less by a third than the flux for the HGm spectrum.

The HGm + KM calculation represents, in fact, a kind of interpolating flux (between QGSJET-II-03 flux and SIBYLL 2.1 one) because the HGm + KM prediction is in close agreement with the HGm + QGSJET one at lower energies and agrees well with HGm + SIBYLL above 100 TeV; the blue bold dot curve and thin magenta one merge into one curve at $E > 200$ TeV (Fig. 4).

Being in close agreement with the IceCube59 measurement data in the energy range from 180 GeV to 36 TeV, the HGm + QGSJET model (only conventional flux) leads to a systematic deviation from the experimental data of the
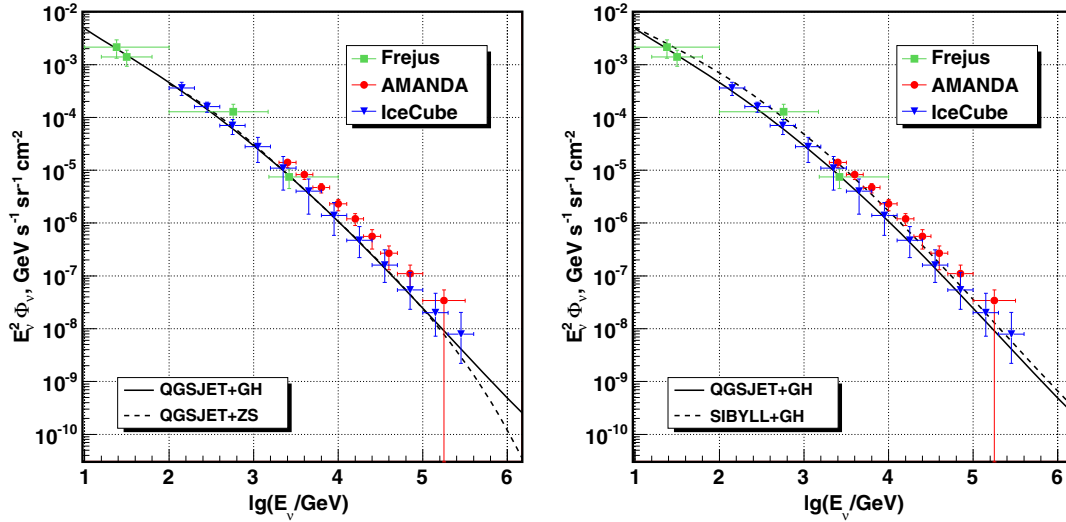
FIG. 2 (color online). Conventional $\nu_\mu + \bar{\nu}_\mu$ spectrum averaged over zenith angles: an influence of the cosmic-ray spectrum "knee" (left panel) and the hadronic model (right). Symbols: data of Frejus [7], AMANDA-II [8], and IceCube [2] experiments.
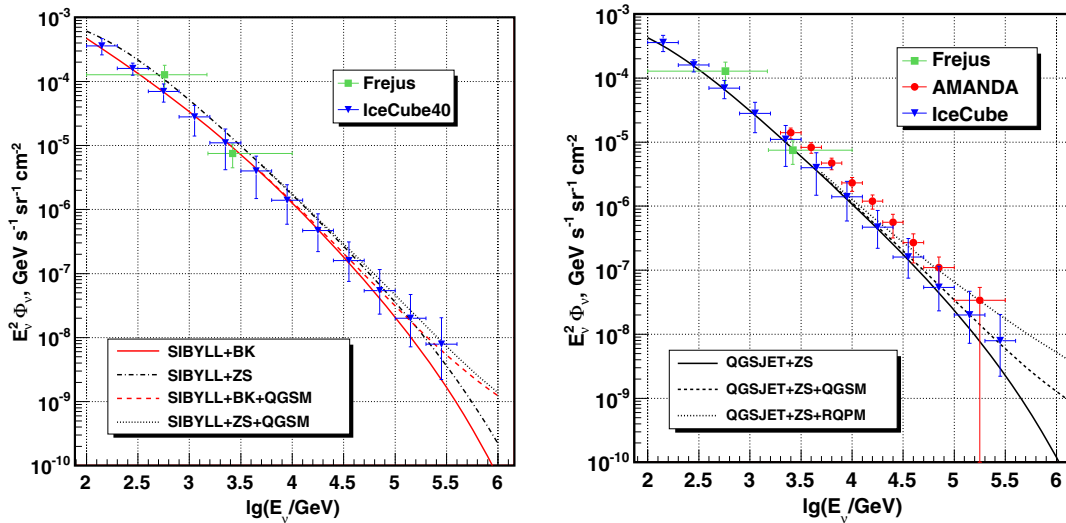

FIG. 3 (color online). Fluxes of the conventional and prompt (QGSM, RQPM) muon neutrinos ($\nu_\mu + \bar{\nu}_\mu$) calculated with use of SIBYLL 2.1 (left panel) and QGSJET-II (right panel) for the cosmic-ray spectrum parametrizations involving the knee.

IceCube59 muon neutrino flux, thus leaving the window for the prompt neutrinos. The HGm + QGSJET + QGSM calculation of the total atmospheric ν_μ flux (blue solid line) may be considered as the preferred model because it describes well the IceCube40 data and gives slightly lowered flux at highest energies reached in the IceCube59 experiment. Similar result gives also the HGm + KM + QGSM model.

Note that possible difference of the calculated conventional $\nu_\mu + \bar{\nu}_\mu$ spectrum, resulting from averaging over the zenith angle range 96°–180° (corresponds to the IceCube40 zenith angle cut, $\theta > 97°$ [2]), which differs from the extended range ($\theta > 88°$) in the IceCube59 analysis [9], really does not exceed 13%.

The atmospheric muon neutrino spectrum reconstructed with the IcuCube59 data reaches energies above 500 TeV where expected is noticeable admixture of the prompt neutrinos and/or the astrophysical. Because the IceCube59 data lead to a higher neutrino spectrum (above 10 TeV) as compared to the IcuCube40 data, there is no compelling evidence against the QGSM prompt neutrino flux prediction, since HGm + QGSJET-II + QGSM gives the total atmospheric $\nu_\mu + \bar{\nu}_\mu$ flux not exceeding the IceCube59 data at the highest energy ($E_\nu = 575$ TeV) if the IceCube astrophysical flux was zero.

On the contrary, if the prompt neutrino flux is the negligible component, then adding the best-fit astrophysical flux [Eq. (15), Sec. IV] to the lowest conventional flux
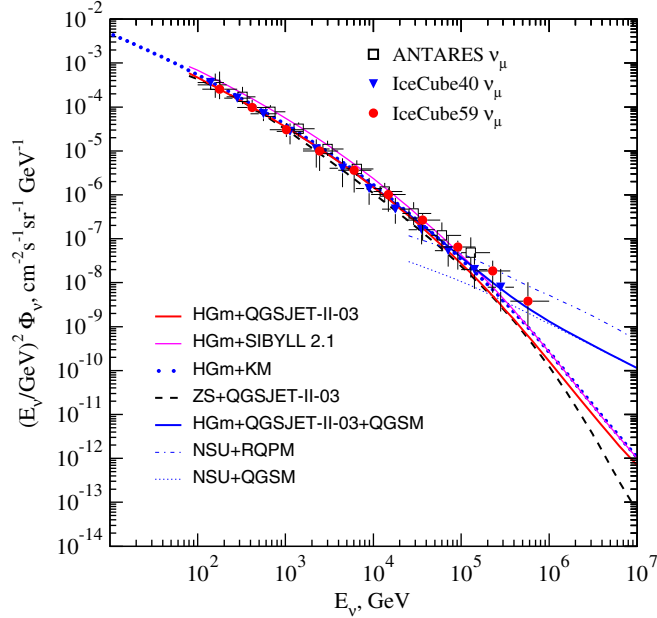
FIG. 4 (color online). The atmospheric $\nu_\mu + \bar{\nu}_\mu$ flux calculations vs the experiment. Conventional flux: HGm + QGSJET (red solid line), HGm + SIBYLL (thin magenta), HGm + KM (bold dots), ZS + QGSJET (dashed). Prompt neutrinos (separately): QGSM (short dash curve), RQPM (dash-dot). Total neutrino flux (sum of the prompt flux and conventional one): HGm + QGSJET + QGSM (blue solid line). The measurement data (symbols): IceCube40 [2], IceCube59 [9] and ANTARES [5].

prediction (ZS + QGSJET) leads evidently to the higher flux at 575 TeV, $\sim 1.0 \times 10^{-8}$ (GeV cm^{-2} s^{-1} sr^{-1}), unlike the value 0.38×10^{-8} in the IceCube59 experiment [9]. Conceivably, this means that the hypothesis of the flavor equipartition ($\nu_e : \nu_\mu : \nu_\tau = 1:1:1$) of the IceCube astrophysical neutrino flux needs a revision (see Refs. [52,53]).

We can describe the conventional zenith-angle-averaged $\nu_\mu + \bar{\nu}_\mu$ flux (due to the prediction of the preferred model, HGm + QGSJET-II) by the approximation valid for 10^2–10^7 GeV with errors not exceeding 12% (at lower energies) (in units of cm^{-2} s^{-1} sr^{-1} GeV^{-1}),

$$\lg[E_\nu^2 \phi_{\nu_\mu}^{\pi,K}(E_\nu)] = -(2.31 + 0.198y + 0.165y^2 \\ + 0.00146y^3), \quad (12)$$

where $y = \lg(E_\nu / 1 \text{ GeV})$. Here we also present the approximation formula describing our calculation (Sec. IV) for the atmospheric conventional $\nu_e + \bar{\nu}_e$ spectrum (the same model, HGm + QGSJET-II-03):

$$\lg[E_\nu^2 \phi_{\nu_e}^{\pi,K}(E_\nu)] = -(2.218 + 0.918y + 0.04899y^2 \\ + 0.00725y^3). \quad (13)$$

Fluxes of neutrinos, Eqs. (12), (13), can be rewritten also in the form

TABLE III. Parameters for the conventional neutrino spectra [Eq. (14)].

Flavor	C_ν	γ_0	γ_1	γ_2
$\nu_\mu + \bar{\nu}_\mu$	4.896×10^{-3}	2.198	1.648×10^{-1}	1.46×10^{-3}
$\nu_e + \bar{\nu}_e$	6.053×10^{-3}	2.918	4.899×10^{-2}	7.25×10^{-3}

TABLE IV. Atmospheric neutrino flux in the energy range (0.4–1) PeV and upper limit for diffuse $\nu_\mu + \bar{\nu}_\mu$ flux obtained with neutrino telescopes.

Model	$E_\nu^2 \phi_\nu$, GeV (cm^2 s sr)$^{-1}$
Conventional $\nu_\mu + \bar{\nu}_\mu$:	$E_\nu = 400$ TeV $-$ 1 PeV
Averaged over angles –	
ZS + SIBYLL 2.1	$(2.21$–$0.214) \times 10^{-9}$
ZS + QGSJET-II	$(1.32$–$0.149) \times 10^{-9}$
BK + QGSJET-II	$(1.09$–$0.097) \times 10^{-9}$
HGm + QGSJET-II	$(1.45$–$0.163) \times 10^{-9}$
Selected zenith angles:	400 TeV–1 PeV
HGm + QGSJET-II, $\cos\theta = 0.5$	$(0.97$–$0.109) \times 10^{-9}$
HGm + QGSJET-II, $\cos\theta = 0.3$	$(1.56$–$0.176) \times 10^{-9}$
HGm + QGSJET-II, $\cos\theta = 0.1$	$(3.40$–$0.384) \times 10^{-9}$
Prompt $\nu_\mu + \bar{\nu}_\mu$:	400 TeV–1 PeV
NSU + QGSM	$(2.90$–$1.16) \times 10^{-9}$
ZS + QGSM	$(2.23$–$0.54) \times 10^{-9}$
$174 E_N^{-3}$ + DM [54]	$(1.87$–$0.85) \times 10^{-9}$
Conv + prompt $\nu_\mu + \bar{\nu}_\mu$:	400 TeV–1 PeV
Conv(averaged) + QGSM	$(4.35$–$1.32) \times 10^{-9}$
Conv(averaged) + DM	$(3.32$–$1.01) \times 10^{-9}$
Conv($\cos\theta = 0.1$) + QGSM	$(6.30$–$1.54) \times 10^{-9}$
Diffuse $\nu_\mu + \bar{\nu}_\mu$:	34.5 TeV–36.6 PeV
IC59 best fit [38]	0.25×10^{-8}
IC59 limit [38]	1.44×10^{-8}
	45 TeV–10 PeV
ANTARES limit [6]	4.8×10^{-8}

$$\phi_\nu^{\pi,K}(E_\nu) = C_\nu \left(\frac{E_\nu}{1 \text{ GeV}} \right)^{-(\gamma_0 + \gamma_1 y + \gamma_2 y^2)}. \quad (14)$$

Two sets of the parameters to Eq. (14) are given in Table III.

The atmospheric muon neutrino fluxes, calculated in the energy range 0.4–1 PeV, are presented also in Table IV along with upper limits on the diffuse flux of astrophysical muon neutrinos obtained in the ANTARES [6] and IceCube59 [38] experiments. The total atmospheric muon neutrino flux (sum of the conventional flux and prompt one) marked in Table IV as "conv. (averaged) + QGSM" is presented by the preferred model HGm + QGSJET-II + QGSM. Note the prompt neutrino flux obtained with the dipole model (DM) [54] is close to the QGSM prediction [50] above 1 PeV (about 30% of the disagreement). More intent inspection of the predicted atmospheric neutrino fluxes, both conventional and prompt, shows that distinctions between the DM

and QGSM prompt muon neutrino flux predictions are hardly observable at the present level of experimental errors if the knee of the cosmic-ray spectrum is thoroughly taken into account.

IV. ELECTRON NEUTRINO FLUX AND THE NEUTRINO FLAVOR RATIO

The sources of the conventional ν_e are three-particle decays of muons μ_{e3} and kaons $K^\pm_{e3}$, K^0_{e3} with the branching ratio 5.07% and 40.5%, respectively. The latter is the dominant source of electron neutrinos at energy below 10 TeV. The semileptonic decays of short-lived K^0_S also contribute though branching ratio of the decay is small (0.07%) [55]. This decay gives a considerable contribution to the atmospheric ν_e flux at high energies, reaching 36% at $E_\nu = 500$ TeV for the zenith angle $\theta = 0°$ (HGm + QGSJET-II model). Close to vertical, the $(\nu_e + \bar{\nu}_e)$ flux from the K^0_S decay becomes nearly equal to that from the K^0_L one at $E_\nu \approx 1$ PeV.

Figure 5 shows the zenith-angle-dependent ν_e flux ratio, $\phi_\nu(E, \theta)/\phi_\nu(E, 0°)$, calculated for $\theta = 90°$ and $72.5°$ with usage of primary spectrum HGm and hadronic interaction models KM, QGSJET-II-03, and SIBYLL 2.1. The curves illustrate partial contributions of kaon sources varying with the energy in accordance with the scale—the critical energy depending on the decay mode and zenith angle: $\epsilon^{cr}_{K^0_L}(\theta = 0°) = 210$ GeV, $\epsilon^{cr}_{K^\pm_{\ell3}}(\theta = 0°) = 890$ GeV, $\epsilon^{cr}_{K^0_S}(\theta = 0°) = 120$ TeV (the critical energy for the horizontal is one order of magnitude larger). The "wave" of zenith-angle enhancement of the atmospheric $(\nu_e + \bar{\nu}_e)$ flux

makes apparent the successive "switching-on" of the kaon sources.

The approximation formula, Eq. (14), describing the calculated zenith-angle-averaged energy spectrum of the atmospheric $\nu_e + \bar{\nu}_e$ flux (HGm + QGSJET-II) was given in Sec. III.

Recently IceCube published results [10] of the first measurement of the atmospheric electron neutrino spectrum in the energy range 80 GeV–6 TeV obtained with the 79-string IceCube configuration including DeepCore. These measurement data make possible an evaluation of the neutrino flavor ratio and comparison it with predictions.

In Fig. 6 we compare the atmospheric $(\nu_e + \bar{\nu}_e)$ flux calculated using QGSJET-II-03 and SIBYLL 2.1 with IceCube measurement data [10] (open triangles) and, in addition, with recent IceCube preliminary data for the atmospheric electron neutrinos [57] (red fill triangles).

The diffuse flux of cosmic neutrinos based on 37 events observed in the IceCube experiment [12,13] is presented in Fig. 6 (the green band and red dash-dot line) with use of the IceCube best fits per flavor, $\phi_\nu \sim E^{-2}$ and $\phi_\nu \sim E^{-2.3}$, borrowed from Ref. [13]:

$$E^2\phi_\nu = (0.95 \pm 0.3) \times 10^{-8} \text{ GeV cm}^{-2}\,\text{s}^{-1}\,\text{sr}^{-1}, \quad (15)$$

$$E^2\phi_\nu = 1.5 \times 10^{-8}(E/100\,\text{TeV})^{-0.3}\,\text{GeV}/(\text{cm}^2\,\text{s sr}). \quad (16)$$
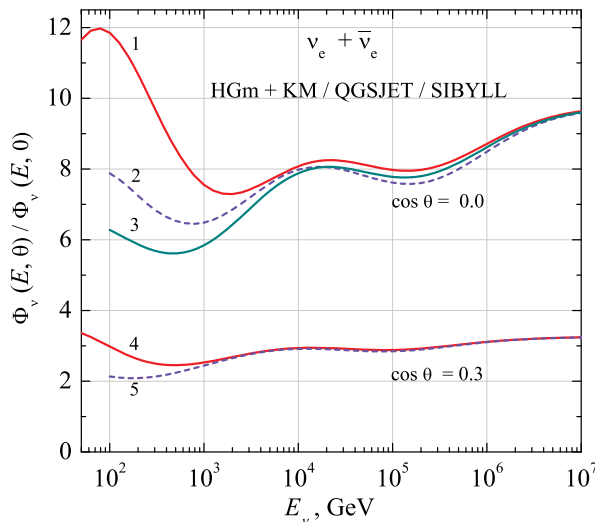

FIG. 5 (color online). Zenith-angle enhancement of the atmospheric $(\nu_e + \bar{\nu}_e)$ flux due to energy alignment of the kaon sources. Curves represent the flux ratio, $\phi_{\nu_e}(\theta)/\phi_{\nu_e}(0°)$, calculated with the HGm primary spectrum for $\theta = 72.5°$, $90°$: 1–KM hadronic model ($90°$), 2–QGSJET-II-03 ($90°$), 3–SIBYLL 2.1 ($90°$), 4–KM ($72.5°$), 5–QGSJET-II-03 ($72.5°$).
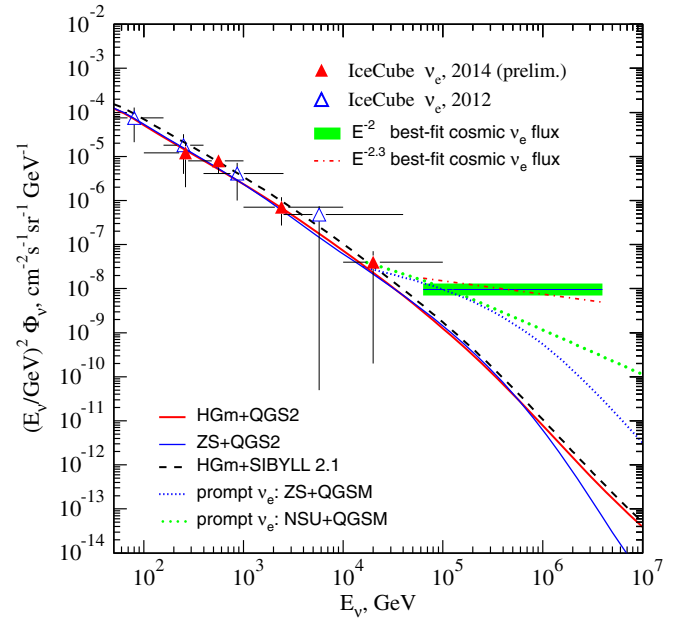

FIG. 6 (color online). Atmospheric $(\nu_e + \bar{\nu}_e)$ spectrum and the diffuse flux of cosmic neutrinos observed in IceCube experiment [13]. The IceCube experimental data: atmospheric neutrinos [10] (triangles) and [57] (filled triangles); the band width reflects the statistical uncertainty of the IceCube best fit for astrophysical neutrino flux [13], Eq. (15); the red dash-dot line corresponds to the IceCube best-fit power law for the astrophysical neutrino spectrum [13], Eq. (16). Curves: predicted fluxes of the atmospheric conventional and prompt neutrinos.

The equal flavor composition ($\nu_e : \nu_\mu : \nu_\tau = 1 : 1 : 1$) and zero prompt neutrino flux were supposed to derive the fits which are valid for deposited energies of neutrino events in the range 60 TeV $< E <$ 3 PeV. The flavor composition of the IceCube astrophysical high-energy neutrino flux is discussed in detail in Refs. [52,53,58–61].

The curves in Fig. 6 correspond to the atmospheric electron neutrino flux, calculated separately for the conventional neutrinos (HGm/ZS + QGSJET/SIBYLL) and prompt ones. The QGSM prompt neutrino flux is represented in Fig. 6 with two curves: green bold dots correspond to the original QGSM flux [50], Eq. (10), and blue short dash line corresponds to that rescaled with the ZS cosmic-ray spectrum. It is clearly seen that the astrophysical ν_e flux and the atmospheric prompt one are competing contributions into detector events at energies above 30–50 TeV.

Since IceCube has measured energy spectra both of muon and electron neutrinos, one can try to construct the neutrino flavor ratio $R_{\nu_\mu/\nu_e} = \phi_{\nu_\mu + \bar{\nu}_\mu}/\phi_{\nu_e + \bar{\nu}_e}$ and check for agreement of the calculation with experimental data. The flavor ratio, being responsive to changes of the electron neutrino flux, reveals an admixture of neutrinos from astrophysical sources or an addition of the atmospheric prompt neutrinos.

The difference in predictions of atmospheric neutrino flux ratio related to choice of hadronic models is seen in Fig. 7: curves display the scale of difference of the

conventional neutrino spectra, calculated with models QGSJET-II, SIBYLL 2.1, and KM for HGm and ZS parametrizations of cosmic-ray spectra (HGm + KM/ QGSJET/SYBILL, ZS + QGSJET). The dashed curve (HKKMS, 2007) in Fig. 7 shows the Monte Carlo calculation by Honda *et al* [62] made with use of the hadronic model DPMJET-III [42,43]; the top curve corresponds to R_{ν_μ/ν_e} calculated with KM hadronic model.

This figure displays the visible difference between the DPMJET-III and KM predictions on the one hand and the QGSJET-II and SIBYLL on the other, which is partly attributable to the difference in the hadronic models in the kaon yield (Table I). The relative proximity of the z factors for KM and DPMJET-III models leads to similar behavior of the neutrino flavor ratio, R_{ν_μ/ν_e} (Fig. 7). However, the R_{ν_μ/ν_e} dissimilarity between SIBYLL and QGSJET-II is not so large as would be expected from the large difference in the kaon production. On the contrary, the same model (QGSJET-II) also leads to visible R_{ν_μ/ν_e} distinction arising from the cosmic-ray spectrum (ZS vs HGm): HGm + QGSJET-II (the curve with dark cyan small squares) and ZS + QGSJET-II (solid red curve).

Relative kaon excess due to KM, DPMJET-III, and SIBYLL makes some kind of "hierarchy" of the plateau in the energy dependence of R_{ν_μ/ν_e} (still corrected for different pion yield):

$$R_{\nu_\mu/\nu_e}^{(QGSJET)} < R_{\nu_\mu/\nu_e}^{(SIBYLL)} < R_{\nu_\mu/\nu_e}^{(DPMJET)} < R_{\nu_\mu/\nu_e}^{(KM)}.$$

Figure 7 also shows a reconstruction of R_{ν_μ/ν_e} derived from the atmospheric neutrino spectra, measured by IceCube [2,10]. Diamonds denote R_{ν_μ/ν_e} values reconstructed with use of the IceCube data [10] and [2], and triangles correspond to the latest preliminary IceCube data for the atmospheric electron neutrino spectrum [57]. The hatched area displays the R_{ν_μ/ν_e} statistical uncertainties of the measurement data:

$$\delta R_{\nu_\mu/\nu_e} = R_{\nu_\mu/\nu_e} \sqrt{(\delta\phi_{\nu_\mu}/\phi_{\nu_\mu})^2 + (\delta\phi_{\nu_e}/\phi_{\nu_e})^2}.$$

To derive ν_μ and ν_e flux values at equal energies, a local interpolation of the experimental data is required. This problem was solved by making the interpolating function (a local fit) for the ν_μ spectrum at energies 100 GeV–20 TeV supported by IceCube40 ν_μ measurement data [2] in the range 141 GeV–35.5 TeV. As the denominator in the $R_{\nu_\mu/\nu_e}(E)$ ratio taken were namely experimental values of the IceCube ν_e flux from Ref. [10], and separately from Ref. [57]. The robustness of the procedure was tested by use, on the contrary, of the ν_μ flux measurement data and a fit for the ν_e spectrum.

In the range 10–100 TeV, our calculations with QGSJET-II and SIBYLL give R_{ν_μ/ν_e} values 17–25
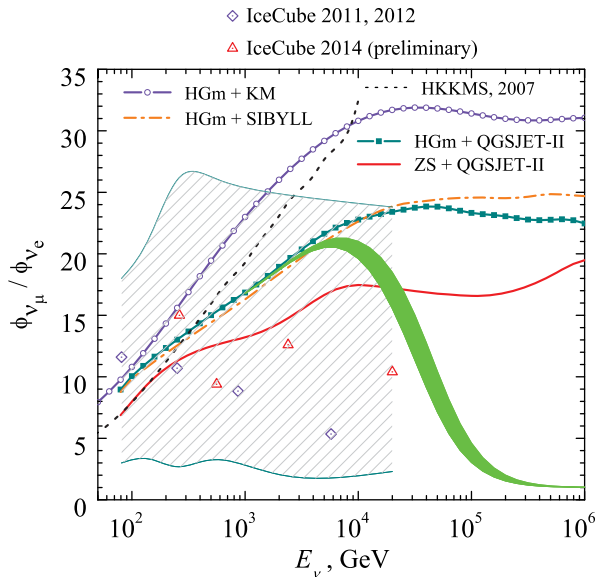

FIG. 7 (color online). The atmospheric neutrino flavor ratio R_{ν_μ/ν_e} calculated for several models in comparison with results derived from IceCube experiments [2,10,57]. Symbols correspond to R_{ν_μ/ν_e} reconstructed from the IceCube measurement data, hatched area images these data uncertainties. The filled green area represents R_{ν_μ/ν_e} obtained for sum of the conventional neutrino flux prediction (HGm + QGSJET) and the best-fit astrophysical neutrino flux [Eq. (15)].

depending on the cosmic-ray spectra (compare ZS + QGSJET-II and HGm + QGSJET-II/SIBYLL, Fig. 7), while the Monte Carlo computation (using CORSIKA) for the same models [39] gives larger values, 25–32.

The hadronic model by Kimel and Mokhov leads to the neutrino flavor ratio R_{ν_μ/ν_e} rather close to the results of Ref. [62] for DPMJET-III [42,43] in the range 100 GeV–10 TeV. In Fig. 7 we see, however, that values of the flavor ratio, like those due to the HGm + KM calculation, $R_{\nu_\mu/\nu_e} \approx 30$ at 10–30 TeV, noticeably exceed not only the R_{ν_μ/ν_e} midpoints (symbols in Fig. 7), reconstructed from IceCube data, but also the hatched area.

The neutrino flavor ratio calculated with the QGSJET-II and SIBYLL 2.1 models agrees on the whole (within statistical and systematic uncertainties) with that reconstructed from IceCube data. However, the IceCube R_{ν_μ/ν_e} midpoints (symbols in Fig. 7) do not reveal a trend toward rising as was expected for the conventional neutrino flux in the energy range 100 GeV–30 TeV. This behavior possibly indicates that the atmospheric electron neutrino flux, measured in the IceCube experiment, contains an admixture of the astrophysical neutrinos in the range 10–30 TeV.

The curved band in Fig. 7 is obtained as a sum of the calculated conventional neutrino flux (HGm + QGSJET-II, zero prompt neutrino flux) and the astrophysical one in accordance with the IceCube best fit [13] [Eq. (15)]. To compute $R_{\nu_\mu/\nu_e}(E_\nu)$ in the range below 60 TeV, the IceCube best fit was extrapolated to 10 TeV. No prompt neutrinos were taken into account. The width of the band reflects the IceCube astrophysical flux uncertainty, $\pm 0.3 \times 10^{-8}$ GeV cm^{-2} s^{-1} sr^{-1}. The extrapolation of the best-fit astrophysical neutrino flux to the energy range below 60 TeV does not contradict R_{ν_μ/ν_e} reconstructed from the IceCube data for atmospheric neutrinos.

In the case of a zero prompt component, the IceCube best-fit astrophysical neutrino flux dominates over the atmospheric $(\nu_e + \bar\nu_e)$ flux at energies above 50 TeV. Close to 50 TeV, the predicted (HGm + QGSJET) atmospheric conventional ν_e flux (scaled by E^2) is about 0.46×10^{-8} GeV cm^{-2} s^{-1} sr^{-1}, which is less than, by half, the best-fit astrophysical flux. An alternative hypothesis, allowing for the prompt neutrino component, leads to similar depression of R_{ν_μ/ν_e} and also might be accepted. However, in this case the prompt neutrino flux should be a rather large one, like the QGSM prediction.

V. SUMMARY

The problem of the atmospheric neutrino background became really important after observation with the IceCube detector of events induced by very high-energy neutrinos of extraterrestrial origin [11–13]. More precise calculations of the high-energy neutrino spectrum are required since it is possible that astrophysical neutrinos are entangled with the atmospheric neutrinos arising from decays of π, K mesons

(conventional neutrinos) and decays of charmed particles (prompt neutrinos) which are produced in collisions of cosmic-ray particles with the Earth's atmosphere.

Presented in this work are the results of the calculations of the high-energy atmospheric neutrino fluxes performed for hadronic interaction models QGSJET-II-03, SIBYLL 2.1, and Kimel and Mokhov, taking into consideration the "knee" of the cosmic-ray spectrum. The calculation shows rather weak dependence on the cosmic-ray spectrum in the energy range 10^2–10^5 GeV. However, the picture appears to be less steady because of a sizable difference in the hadronic model predictions. As can be seen in the example of the models QGSJET-II-03 and SIBYLL 2.1, the major factor in the discrepancy in conventional neutrino fluxes is the kaon production in nucleon-nucleus collisions. Really, cosmic-ray physicists feel the necessity of comprehensive analysis of the actual features of the high-energy hadronic models under discussion, QGSJET-II-03 (04), EPOS-LHC, SIBYLL 2.1, DPMJET-III, especially concerning details of the kaon and charmed particle production in NA, πA collisions.

Above 100 TeV, the calculated spectra of muon neutrinos display an apparent dependence on the spectrum and composition of primary cosmic rays related to the "knee" range. Also in this region, uncertainties appear due to production cross sections and decays of charmed particles which imprint on the prompt neutrino flux.

All calculations are compared with the atmospheric neutrino measurements by Frejus, AMANDA, IceCube, and ANTARES. New reconstruction of the ν_μ spectrum, performed by the IceCube Collaboration [9], seemingly does not map out the QGSM prompt neutrino flux prediction. Being in close agreement with the IceCube measurement data in the energy range from 140 GeV to 100 TeV, the HGm + QGSJET model leads to the systematic deviation from experimental data, especially those for the IceCube59 muon neutrino spectrum in energy in the range 100–500 TeV. Thus, the IceCube59 data leave a window for the QGSM prompt neutrino component: the comparison of the calculation with IceCube measurement data on atmospheric ν_μ and ν_e fluxes makes it possible to consider the HGm + QGSJET-II-03 + QGSM model as the preferable one.

The approximation formula describing the HGm + QGSJET-II-03 predictions of the atmospheric conventional $(\nu_e + \bar\nu_e)$ and $(\nu_\mu + \bar\nu_\mu)$ energy spectra, averaged over zenith angles, is given by Eq. (14). An analytic description of $(\nu_\mu + \bar\nu_\mu)$ and $(\nu_e + \bar\nu_e)$ energy spectra HGm + QGSJET-II-03 can be used, in principle, as one more tool to test data of neutrino event reconstruction in neutrino telescopes.

Authors of the IceCube59 analysis [9] avoid definite conclusions concerning the prompt neutrino contribution or the neutrinos of a cosmic origin because of large systematic uncertainties at the highest energies. Nevertheless, the ν_μ

flux mean values illustrate the state of the problem. Even if the prompt neutrino flux is zero, the sum of the best-fit astrophysical flux and the calculated atmospheric conventional one gives the evidently higher flux compared to the IceCube59 data (the last bin around $E_\nu \approx 575$ TeV). This circumstance gives rise to doubts regarding the equal flavor composition of the IceCucbe astrophysical flux, $\nu_e : \nu_\mu : \nu_\tau = 1 : 1 : 1$.

The IceCube best-fit astrophysical neutrino flux dominates over atmospheric ($\nu_e + \bar{\nu}_e$) flux at energies above 60 TeV (Fig. 6). Around 60 TeV, the highest predicted (HGm + SIBYLL) atmospheric conventional ν_e flux (scaled by E^2) is about 0.5×10^{-8} GeV cm^{-2} s^{-1} sr^{-1}, which is well below the IceCube best-fit astrophysical flux, Eq. (15). Thus, the transition from the atmospheric electron neutrino flux to the predominance of the astrophysical neutrinos occurs at 30–100 TeV if the prompt neutrino component is taken into consideration.

The Kimel and Mokhov hadronic model (HGm + KM) and DPMJET-III [62] lead to rather large values of the atmospheric neutrino flavor ratio in the energy range 10–100 TeV, exceeding those reconstructed from IceCube data. The similar values of the flavor ratio were obtained in the MC computation [39] ($R_{\nu_\mu/\nu_e} \approx 25 - 32$ at $E_\nu = 10 - 100$ TeV, using QGSJET-II and SIBYLL 2.1 models. There is little doubt in this case that a discordance takes place between the calculated R_{ν_μ/ν_e} and the median flavor ratio reconstructed from the IceCube experiment.

At the same time, the neutrino flavor ratio calculated in the present work with QGSJET-II-03 and SIBYLL 2.1 models better agrees (especially for ZS spectrum) with R_{ν_μ/ν_e} reconstructed from the IceCube data. Note, however, that the IceCube midpoints (symbols in Fig. 7) display rather low R_{ν_μ/ν_e} at 1–10 TeV, which does not reveal the trend to increase with energy.

If the power law E^{-2} is valid for the astrophysical neutrino spectrum at energies below 60 TeV, then extrapolation to lower energies of the high-energy neutrino flux, observed in the IceCube experiment [11–13], should lead to decrease of the neutrino flavor ratio R_{ν_μ/ν_e} in the energy range 10–50 TeV. This extrapolation shows the consistency of the ratio R_{ν_μ/ν_e}, calculated with model HGm + QGSJET-II-03, and that obtained from the IceCube data. The computation of the neutrino flavor ratio hints that one more confirmation of the presence of astrophysical neutrinos might be obtained from little progress in measurement of the ν_e spectrum above 20 TeV, because R_{ν_μ/ν_e}, more sensitive to the electron neutrino flux, makes it possible to disclose a small fraction from astrophysical sources.

The neutrino flavor ratio R_{ν_μ/ν_e} extracted from IceCube data does not display a trend toward rising as is expected for the conventional neutrino flux in the energy range 100 GeV–30 TeV (Fig. 7). The R_{ν_μ/ν_e} depression possibly indicates that the atmospheric electron neutrino flux measured in the IceCube experiment contains the admixture of the cosmic neutrinos even in the energy range 10–50 TeV.

[1] V. Aynutdinov *et al.*, Nucl. Instrum. Methods Phys. Res., Sect. A **588**, 99 (2008).

[2] R. Abbasi *et al.* (IceCube Collaboration), Phys. Rev. D **83**, 012001 (2011).

[3] R. Abbasi *et al.* (IceCube Collaboration), Phys. Rev. D **84**, 082001 (2011).

[4] R. Abbasi *et al.* (IceCube Collaboration), Phys. Rev. D **83**, 092003 (2011).

[5] S. Adrian-Martinez *et al.*, Eur. Phys. J. C **73**, 2606 (2013).

[6] V. Van Elewyck (ANTARES Collaboration), Nucl. Instrum. Methods Phys. Res., Sect. A **742**, 63 (2014).

[7] K. Daum *et al.*, Z. Phys. C Part. Fields **66**, 417 (1995).

[8] R. Abbasi *et al.* (IceCube Collaboration), Astropart. Phys. **34**, 48 (2010).

[9] M. G. Aartsen *et al.* (IceCube Collaboration), arXiv:1409.4535v2.

[10] M. G. Aartsen *et al.* (IceCube Collaboration), Phys. Rev. Lett. **110**, 151105 (2013).

[11] M. G. Aartsen *et al.* (IceCube Collaboration), Phys. Rev. Lett. **111**, 021103 (2013).

[12] M. G. Aartsen *et al.* (IceCube Collaboration), Science **342**, 1242856 (2013).

[13] M. G. Aartsen *et al.* (IceCube Collaboration), Phys. Rev. Lett. **113**, 101101 (2014).

[14] R. Laha, J. F. Beacom, B. Dasgupta, S. Horiuchi, and K. Murase, Phys. Rev. D **88**, 043009 (2013).

[15] K. Murase, M. Ahlers, and B. C. Lacki, Phys. Rev. D **88**, 121301(R) (2013).

[16] F. W. Stecker, Phys. Rev. D **88**, 047301 (2013).

[17] O. E. Kalashev, A. Kusenko, and W. Essey, Phys. Rev. Lett. **111**, 041103 (2013).

[18] L. A. Anchordoqui, H. Goldberg, M. H. Lynch, A. V. Olinto, T. C. Paul, and T. J. Weiler, Phys. Rev. D **89**, 083003 (2014); arXiv:1306.5021.

[19] M. Ahlers and F. Halzen, Phys. Rev. D **90**, 043005 (2014); arXiv:1406.2160.

[20] J. Becker Tjus, B. Eichmann, F. Halzen, A. Kheirandish, and S. M. Saba, Phys. Rev. D **89**, 123005 (2014).

[21] W. Winter, Phys. Rev. D **90**, 103003 (2014).

[22] S. Ostapchenko, Phys. Rev. D **74**, 014026 (2006); Nucl. Phys. B, Proc. Suppl. **175–176**, 73 (2008); **151**, 143 (2006).

[23] E. J. Ahn, R. Engel, T. K. Gaisser, P. Lipari, and T. Stanev, Phys. Rev. D **80**, 094003 (2009); R. S. Fletcher, T. Gaisser, P. Lipari, and T. Stanev, Phys. Rev. D **50**, 5710 (1994).

[24] A. A. Kochanov, T. S. Sinegovskaya, and S. I. Sinegovsky, Astropart. Phys. **30**, 219 (2008).

[25] A. A. Kochanov, T. S. Sinegovskaya, and S. I. Sinegovsky, J. Exp. Theor. Phys. **116**, 395 (2013); Zh. Eksp. Teor. Fiz. **143**, 459 (2013).

[26] A. N. Kalinovsky, N. V. Mokhov, and Yu. P. Nikitin, *Passage of High-Energy Particles through Matter* (American Institute of Physics, New York, 1989).

[27] V. I. Zatsepin and N. V. Sokolskaya, Astron. Astrophys. **458**, 1 (2006).

[28] A. M. Hillas, arXiv:astro-ph/0607109v2.

[29] T. K. Gaisser, Astropart. Phys. **35**, 801 (2012).

[30] D. Bindig, C. Bleve, and K.-H. Kampert, in *Proceedings of 32nd International Cosmic Ray Conference, Beijing, 2011*, edited by H. Hu (Institute of High Energy Physics, Beijing, 2011), Vol. 1, p. 161.

[31] J. Horandel, Astropart. Phys. **19**, 193 (2003); **21**, 241 (2004).

[32] V. A. Naumov and T. S. Sinegovskaya, Phys. At. Nucl. **63**, 1927 (2000).

[33] S. I. Sinegovsky, A. A. Kochanov, T. S. Sinegovskaya, A. Misaki, and N. Takahashi, Int. J. Mod. Phys. A **25**, 3733 (2010).

[34] A. C. Genz and A. A. Malik, J. Comput. Appl. Math. **6**, 295 (1980).

[35] T. Antoni *et al.*, Astropart. Phys. **24**, 1 (2005).

[36] A. D. Panov *et al.*, Bull. Russ. Acad. Sci. Phys. **71**, 494 (2007); **73**, 564 (2009).

[37] H. S. Ahn *et al.*, Astrophys. J. Lett. **714**, L89 (2010); Astrophys. J. **707**, 593 (2009).

[38] M. G. Aartsen *et al.* (IceCube Collaboration), Phys. Rev. D **89**, 062007 (2014).

[39] A. Fedynitch, J. Becker Tjus, and P. Desiati, Phys. Rev. D **86**, 114024 (2012).

[40] G. Fiorentini, V. A. Naumov, and F. L. Villante, Phys. Lett. B **510**, 173 (2001).

[41] V. A. Naumov, in *Proceedings of the 2nd Workshop on Methodical Aspects of Underwater/Underice Neutrino Telescopes*, edited by R. Wischnewski (DESY, Hamburg, 2002), arXiv:hep-ph/0201310v2.

[42] S. Roesler, R. Engel, and J. Ranft, arXiv:hep-ph/0012252.

[43] T. Sanuki, M. Honda, T. Kajita, K. Kasahara, and S. Midorikawa, Phys. Rev. D **75**, 043005 (2007).

[44] L. Derome, Phys. Rev. D **74**, 105002 (2006).

[45] T. K. Gaisser and M. Honda, Annu. Rev. Nucl. Part. Sci. **52**, 153 (2002).

[46] S. I. Sinegovsky, O. N. Petrova, and T. S. Sinegovskaya, in *Proceedings of 32nd International Cosmic Ray Conference, Beijing, 2011*, edited by H. Hu (Institute of High Energy Physics, Beijing, 2011), Vol. 4, p. 300; arXiv:1109.3576.

[47] O. N. Petrova, T. S. Sinegovskaya, and S. I. Sinegovsky, Phys. Part. Nucl. Lett. **9**, 766 (2012).

[48] S. I. Sinegovsky, E. V. Ogorodnikova, and T. S. Sinegovskaya, in *Proceedings of 33rd International Cosmic Ray Conference, Rio de Janeiro, 2013*, arXiv:1306.5907v2.

[49] A. B. Kaidalov and O. I. Piskunova, Sov. J. Nucl. Phys. **41**, 816 (1985); **43**, 994 (1986); Z. Phys. C **30**, 145 (1986).

[50] E. V. Bugaev, V. A. Naumov, S. I. Sinegovsky, and E. S. Zaslavskaya, Nuovo Cimento C **12**, 41 (1989).

[51] S. I. Nikolsky, I. N. Stamenov, and S. Z. Ushev, Zh. Eksp. Teor. Fiz. **87**, 18 (1984) [Sov. Phys. JETP **60**, 10 (1984)].

[52] O. Mena, S. Palomares-Ruiz, and A. C. Vincent, Phys. Rev. Lett. **113**, 091103 (2014).

[53] A. Watanabe, arXiv:1412.8264.

[54] R. Enberg, M. H. Reno, and I. Sarcevic, Phys. Rev. D **78**, 043005 (2008).

[55] It should be noted that the contribution of semileptonic decay $K_S^0 \to \pi e \nu_e$ into the atmospheric ν_e flux was taken into account long ago [41], contrary to the assertion in Ref. [56]: "We have identified a hitherto overlooked contribution to the conventional atmospheric ν_e flux, from $K_S \to \pi e \nu_e$." Since 1999 calculations of the atmospheric electron neutrino flux included this source by default after T. Sinegovskaya, PhD thesis, Irkutsk State University, 1999, and V. Naumov [41]. The citation from Ref. [41] (p. 12): "The high-energy calculation takes into account many thin effects, like K_{e3} and $K_{\mu3}$ form factors and K_S^0 semileptonic decays, meson regeneration, and charge exchange through reactions $\pi^\pm + \mathrm{Air} \to \pi^{\pm(\mp)} + X$ $\pi^\pm + \mathrm{Air} \to K^{\pm(0)} + X$, etc., as well as through $K_{\pi2}$ and $K_{\pi3}$ decays." The latest calculations of atmospheric ν_e flux [46–48] also included the K_S^0 semileptonic decay.

[56] T. K. Gaisser and S. R. Klein, Astropart. Phys. **64**, 13 (2015).

[57] G. Binder, in Proc. of 18th ISVHECRI, 2014, CERN, Geneva (unpublished), https://indico.cern.ch/event/287474/other-view?view=standard.

[58] D. Fargion and P. Paggi, Nucl. Instrum. Methods Phys. Res., Sect. A **753**, 9 (2014).

[59] L. Fu and C. Man Ho, arXiv:1407.1090v2.

[60] X.-J. Xu, H.-J. He, and W. Rodejohann, J. Cosmol. Astropart. Phys. 12 (2014) 039.

[61] C.-Y. Chen, P. S. Bhupal Dev, and Amarjit Soni, arXiv:1411.5658v2.

[62] M. Honda, T. Kajita, K. Kasahara, S. Midorikawa, and T. Sanuki, Phys. Rev. D **75**, 043006 (2007).